Journal of Constructional Steel Research 166 (2020) 105904

Contents lists available at ScienceDirect

Journal of Constructional Steel Research

Residual stresses of box and I-shaped columns fabricated from S960 ultra-high-strength steel

Dongxu Li [a,*], Anna Paradowska [a,b], Brian Uy [a], Jia Wang [a], Mahbub Khan [a,b]

[a] School of Civil Engineering, The University of Sydney, Sydney, NSW 2006, Australia
[b] Australian Centre for Neutron Scattering ANSTO, Lucas Heights, NSW 2234, Australia

ARTICLE INFO

Article history:
Received 9 July 2019
Received in revised form 29 November 2019
Accepted 9 December 2019
Available online 24 December 2019

Keywords:
Residual stresses
UHSS
Box and I-shaped columns
Non-destructive
Neutron diffraction
Analytical model

ABSTRACT

Ultra-high-strength steel (UHSS) with a nominal yield stress of 960 MPa is of significant interest for the design of heavily loaded compressive members, such as high-rise buildings, long-span bridges and large-scale infrastructure. However, the residual stresses induced by the fabrication process can be detrimental to the structural members. In particular, compressive residual stresses can result in premature buckling and the ultimate strength of fabricated columns will be reduced. To date, research pertaining to the distribution of the residual stresses for UHSS column is limited. An experimental program about the measurements of residual stress distributions for UHSS box and I-shaped columns is therefore presented herein. Measurements of residual stress were undertaken on two box and two I-shaped columns having various width-to-thickness ratios by using the non-destructive neutron diffraction method. The distributions of residual stress in three orthogonal directions for each specimen was measured. The influences of column width-to-thickness ratio on residual stress distributions were investigated and discussed. In addition, simplified analytical models for the box and I-shaped column were established to facilitate the buckling analysis for such UHSS columns. Comparisons of the residual stress distributions between the experimental results and analytical model demonstrated a good agreement and this model can be safely used for the fabricated high-strength-steel (HSS) and UHSS column.

Crown Copyright © 2019 Published by Elsevier Ltd. All rights reserved.

1. Introduction

High-performance steels have been available for more than two decades [1]. However, due to the high manufacturing cost, reduced ductility performance and lack of rational design guidance, the wider application of high-strength steel (HSS) and ultra-high-strength steel (UHSS) in engineering practice has been very limited. Recently, an increasing interest in taller and longer building structures has made high-performance steel an ideal substitute for structural applications again [2]. These high-performance materials allow more economic and sustainable building structures to be achieved, which are of major importance to an overall project [3]. Steel columns that are fabricated from HSS and UHSS plates possess excellent mechanical properties and have attracted the attention from many researchers. Previous research [4–8] reported experimental results of fabricated HSS and UHSS box and I-shaped columns under various loading combinations, the nominal yield stresses of structural steels ranged from 690 to 960 MPa. In addition to the studies on bare steel columns, HSS and UHSS have been used as the outer steel tubes to form composite members with infilled concrete. The investigations of slenderness limits and ultimate strength for composite columns incorporating high-performance materials under different loading conditions have been carried out extensively [9–18].

Residual stress has a wide range of undesirable effects on the structural elements. Specifically, tensile residual stress might result in premature crack and affect the fatigue behaviour, which consequently lead to structural failure [19,20]. Moreover, the existence of compressive residual stress may lead to premature buckling and reduce the ultimate strength capacity of the axially loaded columns [21–23]. To avoid over-prediction of the ultimate strength, comprehensive and accurate investigation of residual stress distributions of various fabricated steel columns need to be conducted. Over the past few decades, many methodologies have been developed for the residual stress measurement and these methods can be normally categorised as destructive and non-destructive [24]. The most commonly used destructive techniques for residual stress measurement include sectioning and hole-drilling method [25]. In particular, the width of steel strip is normally taken as 8–15 mm for sectioning method, which could lead to a large averaging volume for the measurement and consequently result in a lower tensile residual stress near the welds. However, the non-destructive technique normally have ability to investigate the stresses in those critical locations, these methods include ultrasonic and X-ray, as well as synchrotron and neutron diffraction. Compared with lab X-ray, synchrotron

* Corresponding author.
E-mail address: dongxu.li@sydney.edu.au (D. Li).

https://doi.org/10.1016/j.jcsr.2019.105904
0143-974X/Crown Copyright © 2019 Published by Elsevier Ltd. All rights reserved.

X-ray and ultrasonic methods, neutron diffraction technique allow neutrons to penetrate deep into the test specimens [26]. By using the Kowari strain scanner at Australia's Nuclear Science and Technology Organisation (ANSTO), the neutrons can penetrate steel plates with thickness from 1 mm up to 50 mm. It should be noted that one of the most significant benefits of using UHSS is the reduced structural dimension. Therefore, four UHSS sections that are fabricated from thin plates of 5 mm is measured in this experimental program.

Over the past few years, an increasing number of studies into residual stress measurement for HSS columns have been performed. Extensive experimental programs [27–37] concerning the residual stresses in the fabricated HSS box, I- and octagonal-shaped columns have been performed. The nominal yield stresses of the measured specimens ranged from 460 to 690 MPa. By comparison, very scarce experimental programs have been conducted to measure the residual stresses of UHSS columns [38–40]. It should be noted that all the previous studies into residual stress patterns for high-strength structural steel columns were performed with the destructive method, either in sectioning method or hole-drilling method. Only the previous research by Khan et al. [31] was conducted with neutron diffraction method, which aims to investigate the S690 HSS box sections only. The present study, however, attempts to investigate the residual stress of the S960 UHSS box and I-sections.

The research on residual stress distributions of UHSS columns through accurate and non-destructive techniques is insufficient. The authors thus presented the experimental results on residual stress distributions for two box and two I-shaped columns fabricated from UHSS plates, which differed in width-to-thickness ratios. A simplified model was proposed to describe the residual stress distributions for HSS and UHSS fabricated box and I-shaped columns.

2. Non-destructive neutron diffraction method

2.1. Introduction

The Bragg Law is employed to provide information on the lattice spacing d_{hkl}, which can be used as a strain gauge to identify the lattice deformation due to the applied residual stresses [41,42]. It should be noted that the Kowari strain scanner utilised in the present study is built on OPAL reactor and single lattice spacing. Based on Bragg's Law equation, the lattice spacing, d_{hkl}, and its variation can be expressed as:

$$n\lambda = 2d_{hkl}\ sin\theta \tag{1}$$

where n was an integer, λ and θ was the wavelength and diffracted angle, respectively (Fig. 1(a)). With a given wavelength and d_{hkl0} under the stress-free condition, the elastic strain due to the residual stress can be expressed as below [43]:

$$\varepsilon = \frac{d_{hkl} - d_{hkl0}}{d_{hkl0}} = -\cot\theta_{hkl}(\theta_{hkl} - \theta_{hkl0}) \tag{2}$$

As suggested by [44,45], it is necessary to measure the strains in three orthogonal directions (x, y and z) for any measuring point. The

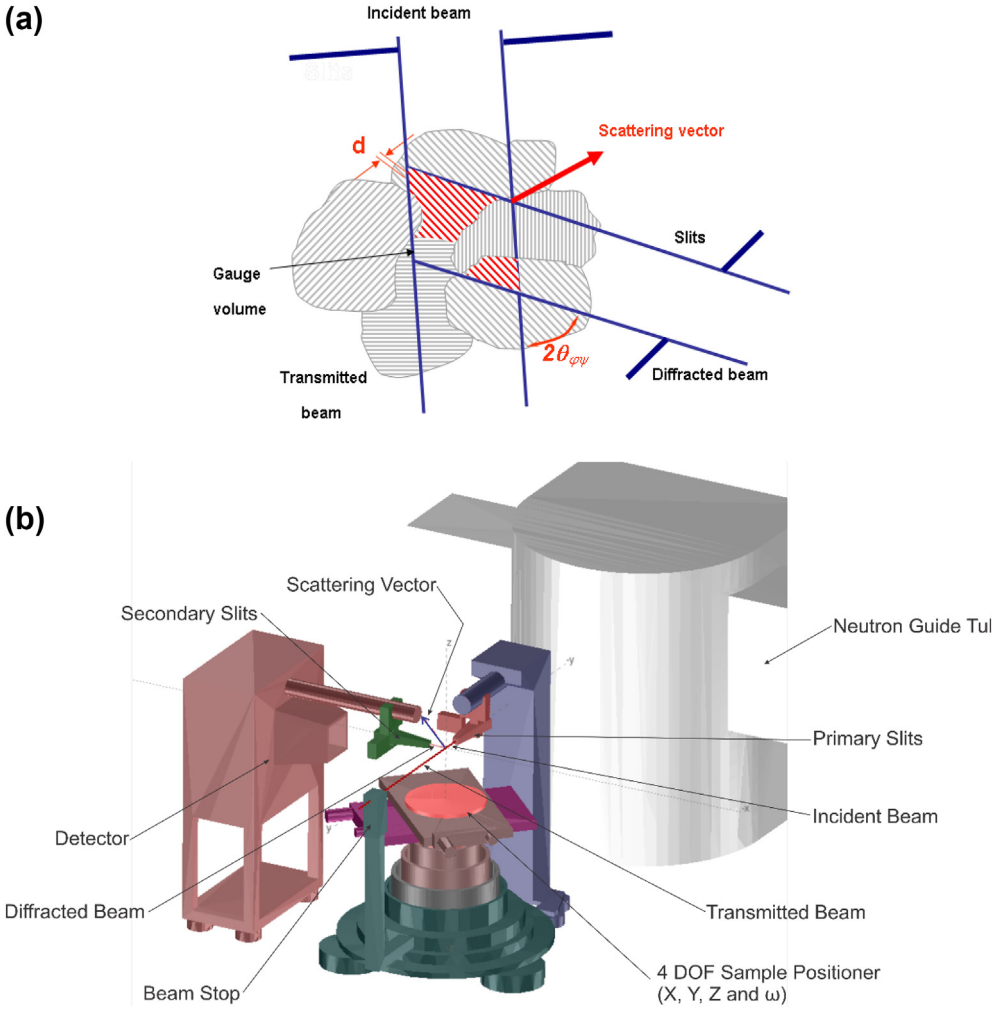

Fig. 1. (a). Principle of neutron diffraction. (b). Schematic of the Kowari strain scanner.

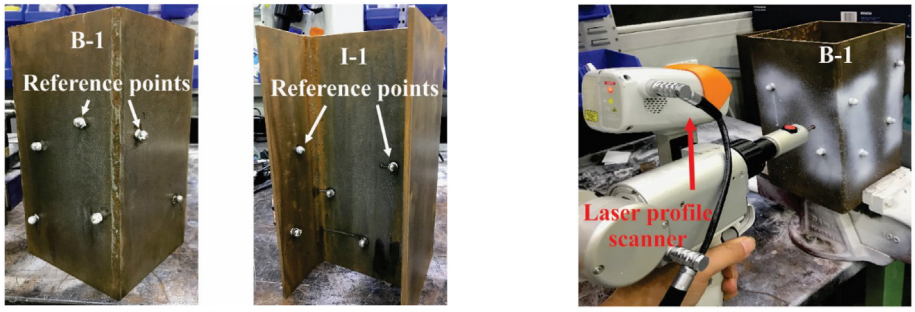

(a) Installation of reference points (b) Laser profile scanning

Fig. 2. Coordinate measurements.

stress components, σ_x, σ_y and σ_z, can then be calculated using the generalised Hooke's law:

$$\sigma_x = \frac{E}{1+\nu}\left(\varepsilon_x + \frac{\nu}{1-2\nu}(\varepsilon_x+\varepsilon_y+\varepsilon_z)\right) \quad (3)$$

$$\sigma_y = \frac{E}{1+\nu}\left(\varepsilon_y + \frac{\nu}{1-2\nu}(\varepsilon_x+\varepsilon_y+\varepsilon_z)\right) \quad (4)$$

$$\sigma_z = \frac{E}{1+\nu}\left(\varepsilon_z + \frac{\nu}{1-2\nu}(\varepsilon_x+\varepsilon_y+\varepsilon_z)\right) \quad (5)$$

with E and ν being Young's modulus and Poisson's ratio of UHSS, and are taken as 204 GPa and 0.3, respectively.

2.2. Accuracy of the neutron diffraction method

As suggested by [46,47], many parameters or sources can contribute to the measurement uncertainties of lattice spacing d_{hkl} and d_{hk0}, such as the peak position and texture effects. In the present study, measurement uncertainties were characterised by an error propagation method [48], which considered uncertainties for the measured specimens. The uncertainties of a stressed component in three orthogonal directions were expressed through Eqs. [6–8]:

$$\Delta\sigma_x = C_1\sqrt{C_2(\Delta\varepsilon_x)^2 + C_2{}^2\left((\Delta\varepsilon_x)^2 + (\Delta\varepsilon_y)^2 + (\Delta\varepsilon_z)^2\right)} \quad (6)$$

$$\Delta\sigma_y = C_1\sqrt{C_2(\Delta\varepsilon_y)^2 + C_2{}^2\left((\Delta\varepsilon_x)^2 + (\Delta\varepsilon_y)^2 + (\Delta\varepsilon_z)^2\right)} \quad (7)$$

$$\Delta\sigma_z = C_1\sqrt{C_2(\Delta\varepsilon_z)^2 + C_2{}^2\left((\Delta\varepsilon_x)^2 + (\Delta\varepsilon_y)^2 + (\Delta\varepsilon_z)^2\right)} \quad (8)$$

where C_1 and C_2 were constants and equal to $E/(1+\nu)$ and $\nu/(1\text{-}2\nu)$, respectively.

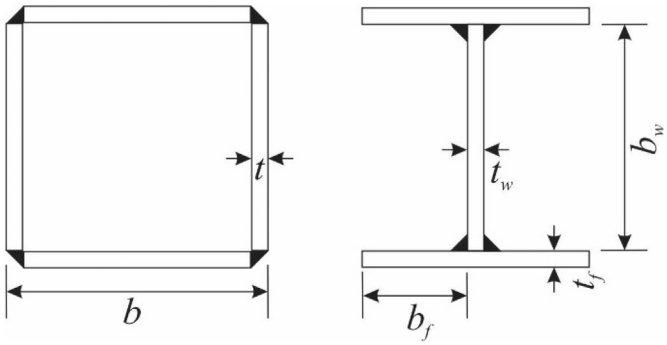

Fig. 3. Schematic view of the test specimens.

2.3. Kowari strain scanner

The neutron scattering facility utilised in the present study is the Kowari strain scanner at ANSTO, which is built on the OPAL reactor. The schematic of the Kowari strain scanner was shown in Fig. 1(b). The experimental procedure was described in details in the author's previous work [31]. To optimise the stress measurements, Kowari virtual machine was used to accurately identify the spatial coordinates of each tested points, as shown in Fig. 2.

3. Experimental programme

3.1. Fabrication of stressed samples

Two box and two I-shaped columns are fabricated for the present study and the configuration details are illustrated in Fig. 3 and Table 1. All component plates are fabricated from UHSS plates of 5 mm thickness and the chemical compositions of the steel plates are shown in Table 2. The UHSS plates were preheated to 50 °C prior to the single pass fillet welding. In particular, the weld consumable utilised herein is ER110S welding wire, whose yield strength (close to 700 MPa) is lower than that of base metal. No specific post-heat treatment was performed after the fillet welding. Gas metal arc welding (GMAW) with a welding velocity of 150 mm/min was used to fabricate these four columns, where the voltage and electric current of the welding was around 25 V and 120 A, respectively.

3.2. Preparation of stress-free reference samples

For the purposes of calculating residual stresses, it is also imperative to prepare and measure stress-free reference sample. Stress-free reference samples were wire-cut as small slices from each of the measured UHSS section across the weld, where the specimens were fully

Table 1
General information of the specimens.

Specimens	Section type	b (mm)	b_f (mm)	b_w (mm)	t (mm)	b/t	b_f/t	b_w/t	L (mm)
B-1	Box	150	–	–	5	30	–	–	450
B-2		250	–	–	5	50	–	–	750
I-1	I-shaped	–	75	140	5	–	15	28	450
I-2		–	125	240	5	–	25	48	750

Table 2
Chemical compositions of the 5 mm UHSS plate provided by steel supplier.

Weight (%)	C	P	Mn	Si	S	Cr	Mo	B	CE (IIW)	CET
	0.18	0.025	1.2	0.25	0.008	0.25	0.25	0.002	0.40	0.29

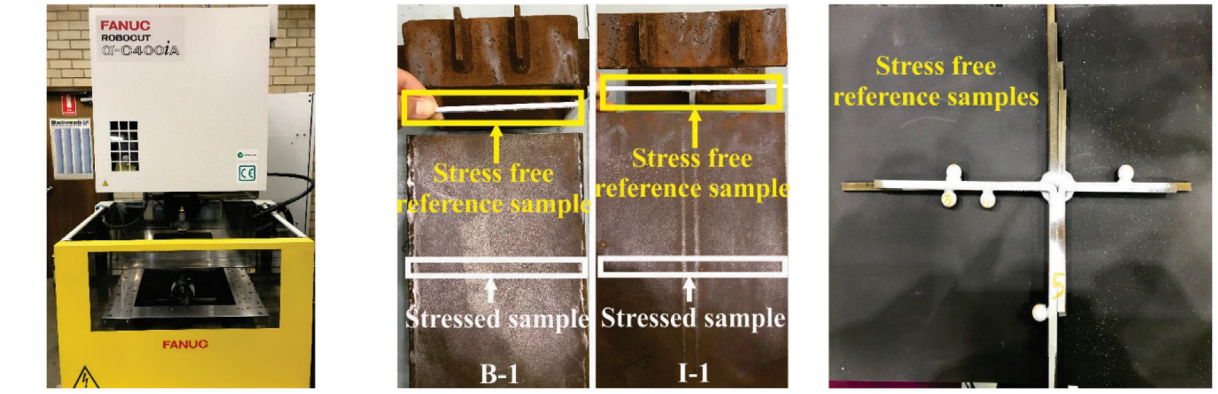

Fig. 4. Preparation of the stress-free reference samples.

immersed in the coolant and no internal stresses were consequently induced. These cuts were made in the perpendicular direction to the welding as shown in Fig. 4(b), with an aim of releasing the residual stresses in the most dominant directions. As measured, there is no significant variation in terms of the lattice spacing from the base metal to the HAZ and weld.

3.3. Virtual simulations of the measured samples

Both the stressed and stress-free reference samples need to be scanned with a laser scanner machine prior to the actual measurements. The virtual simulations of the measured samples were generated by using a coordinate measuring machine (CMM). As shown in Fig. 2(a) and Fig. 4(c), the reference points were installed on the measured samples to align the virtual simulation with the experimental setup on Kowari. The procedure was described in details in authors' previous work [31,49]. This virtual simulation procedure also determined the measuring points' location for each stressed and stress-free reference sample. The distance of measuring points away from the critical welded region increased from 2.5 mm and 5 mm to 15 mm (Fig. 5).

3.4. Experimental set-up for neutron diffraction measurement

The tested specimens were mounted on the translational table accurately with the assistance of reference points, which ensured the precise positioning of the experimental gauge volume for planned neutron measurements. The translational table and measured samples were controlled and positioned so the cubic gauge volume was achieved, as shown in Fig. 6. In order to maintain the measuring accuracy whilst maximise measurement efficiency, optimal gauge volume size of $2 \times 2 \times 2$ mm^3 is adopted, which is only 20% of that through sectioning method. The error of measurements along three orthogonal directions ($\Delta\sigma_x$, $\Delta\sigma_y$, $\Delta\sigma_z$) is obtained through Eqs. (6-8) respectively. The averaged measurement error of 28 MPa along weld longitudinal direction is obtained and below 5% of the yield strength of the parent metal.

4. Test results and discussion

4.1. Coupon tests

In order to identify the residual stress distribution for UHSS column as a function of its yield stress, a series of coupons extracted from the spare fabricated specimens were tested according to AS 1391 [50]. A typical full-range stress-strain relationship of UHSS is plotted in Fig. 7. From the tensile coupon tests, the average yield and ultimate stress of the UHSS plate is determined as 970 MPa and 1030 MPa, as shown in Table 3.

4.2. Measurement results of box columns

In the present study, nearly 700 measurements along three orthogonal directions of 230 measuring points are taken to establish the residual stress distributions for fabricated UHSS box columns. Specifically, the stressed lattice spacing d_{hkl} is measured and the corresponding residual strains and stresses along three orthogonal directions (ε_x, ε_y, ε_z

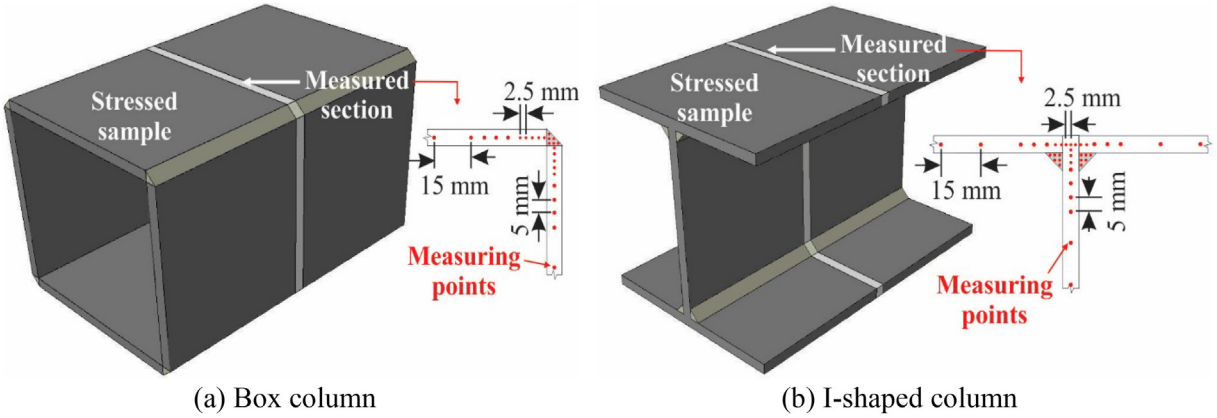

Fig. 5. Illustration of measuring points.

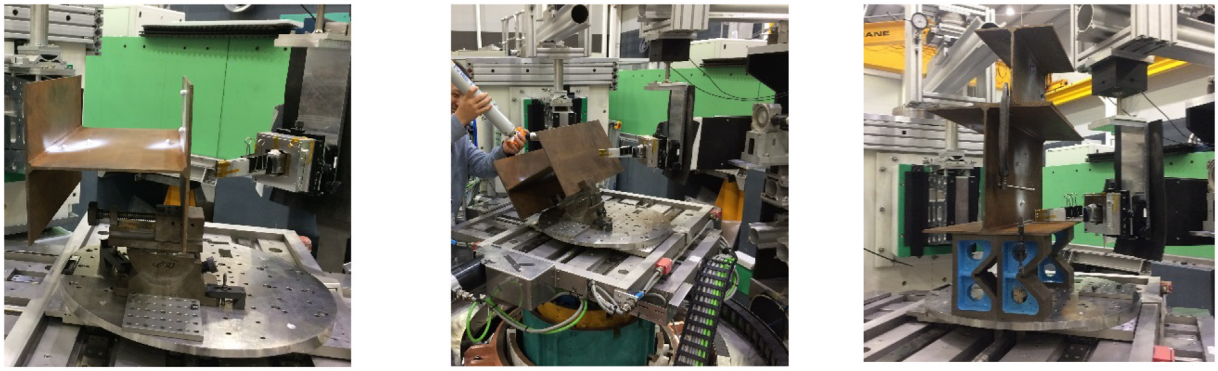

Fig. 6. Experimental set-up for I-shaped columns of different measuring angles.

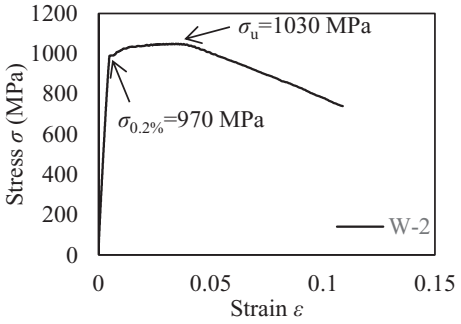

Fig. 7. A typical full stress-strain relationship of UHSS.

Table 3
Tensile coupon test results for UHSS.

Coupons	Young's modulus, E (GPa)	0.2% proof stress, $\sigma_{0.2\%}$ (MPa)	Ultimate stress, σ_u (MPa)
B-1	204.4	981.0	1042.4
B-2	201.1	985.2	1033.2
F-1	208.4	976.7	1034.4
F-2	198.6	957.6	1022.0
W-1	209.1	955.7	1020.8
W-2	203.8	968.2	1030.4

and σ_x, σ_y, σ_z) can be obtained through Eqs. [2–5]. For each UHSS section, the maximum tensile residual stress is simply taken from the measured results, which is not located at the weld centre but close to the heat affected zone. The potential reason is explained with details in Section 4.6. In addition to the identification of the maximum tensile residual stress, the averaged tensile residual stress is of more interests in the present study, as this averaged tensile residual stress can facilitate the development of complete residual stress pattern. Specifically, the averaged tensile residual stress for each UHSS section is determined by counting and averaging all the points that are within 12 mm from the weld centre, where the tensile residual stress exists. On the other hand, the averaged compressive residual stress is determined through the remaining points by removing those with significant measurement error ($\Delta\sigma_z > 50$ MPa). The self-equilibrium is checked for the UHSS sections measured in the present study. The residual stress magnitude and distribution pattern of the top component plate for box column B-1 was presented in Fig. 8(a). The residual stresses of the selected component plates in three orthogonal directions show that the longitudinal residual stresses are dominant; whilst the highest stress in transverse and normal directions is below 30% of the yield strength of the parent metal. Considering the steel and composite columns are mainly subjected to axial loading and are more affected by the longitudinal residual stresses, the following Fig. 9 only presented the longitudinal residual stress distribution patterns for box columns.

As observed, the trend of residual stress distributions is similar to that of conventional HSS box columns [38–40]. Specifically, almost constant compressive residual stresses of −110 MPa and −55 MPa exist over the component plates of B-1 and B-2, respectively. Moreover, the maximum and average tensile residual stresses in the vicinity of welds are around 850 MPa and 730 MPa, respectively, which are significantly higher than those obtained through the sectioning method. This discrepancy is mainly due to the inherent shortcomings of the sectioning method, where larger gauge volumes are used for measurement and the maximum tensile residual stress near the weld bead region is averaged and significantly underestimated. As observed, the normalised tensile residual stress (σ_{rt}/f_y) for UHSS box columns (0.72) is similar to that of lightly welded HSS columns [31].

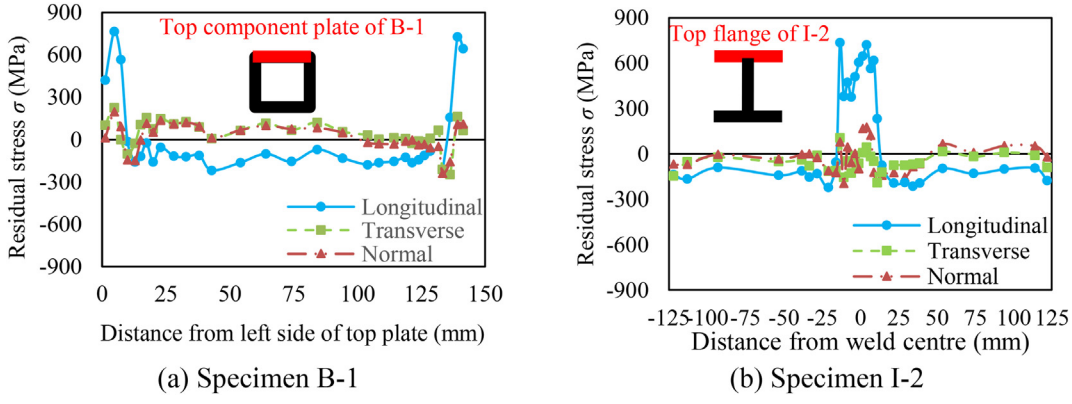

Fig. 8. Residual stress distribution of selected component plates.

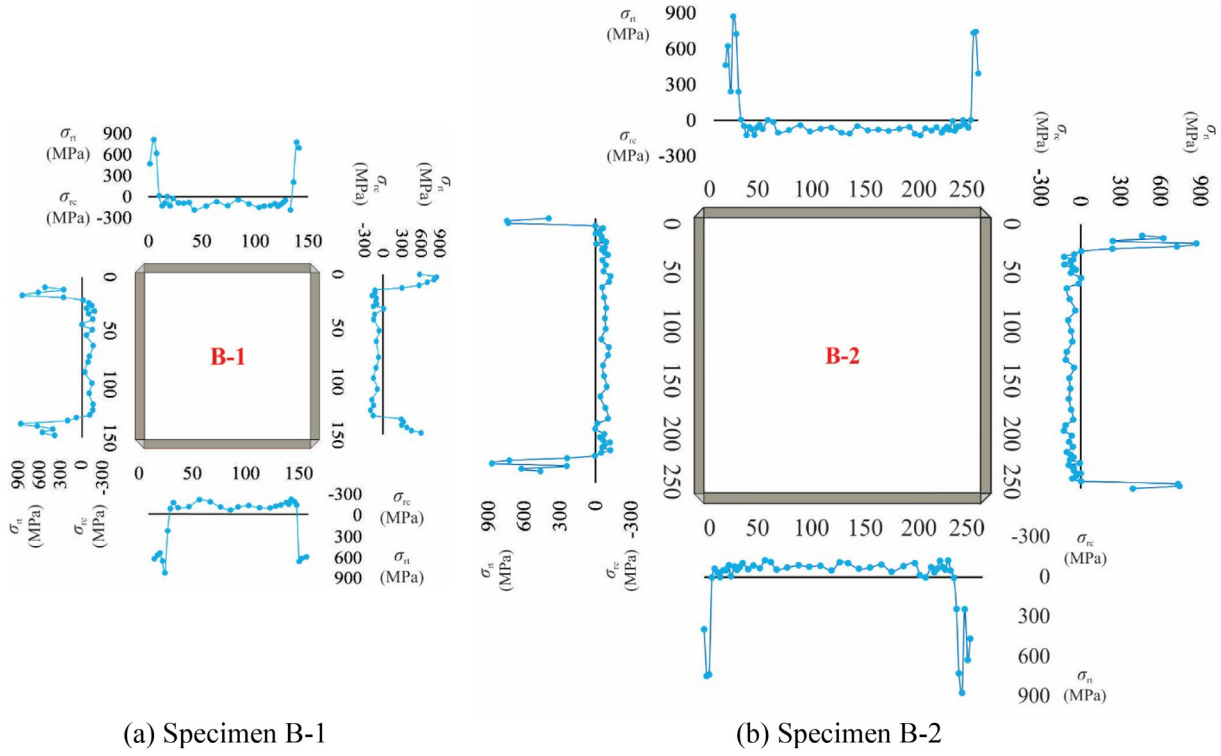

Fig. 9. Longitudinal residual stresses of fabricated UHSS box columns.

Furthermore, a characterised residual stress distribution pattern for UHSS box column is illustrated in Fig. 10(a) and summarised in Table 4, where $\sigma_{rc1}-\sigma_{rc4}$ and $\sigma_{rt1}-\sigma_{rt8}$ represents the average compressive and tensile residual stresses, respectively.

4.3. Measurement results of I-shaped columns

The UHSS I-shaped columns were measured at 150 measuring locations to establish the residual stress distributions. Fig. 8(b) presents the normal, transverse and longitudinal residual stress distributions of the top flange plate for Specimen I-2. Similarly, Fig. 11 only presents the longitudinal residual stresses for Specimens I-1 and I-2.

In the present study, nearly constant compressive residual stresses of −240 MPa and −110 MPa over the flange plates of I-1 and I-2 are observed, which are different from the results reported in previous studies [28,29]. This discrepancy is mainly attributed to the use of different cutting techniques. The UHSS plates utilised herein are cut with a waterjet machine, whilst the specimens from studies in [28,29] are flame cut and additional tensile residual stresses at the edges of the flange plates are inevitably produced. Moreover, the maximum and average tensile residual stresses are around 810 MPa and 710 MPa, respectively, which are higher than that from conventional mild steel and HSS columns.

To facilitate the utilisation of structural engineers, the residual stress distributions for UHSS I-shaped columns are shown in Fig. 10(b) and the measured values are summarised in Table 5.

4.4. Residual stresses of the welds

Owing to the unique benefits of the non-destructive high spatial resolution neutron diffraction measurement technique, the measuring points can be taken at the regions of rapid change in stress such as welds and HAZ, where sectioning method have a significant limitations. Fig. 12 illustrates the measured residual stresses at the weld and the HAZ for Specimens B-1 and I-1. Generally, the tensile residual stresses are localised within the vicinity of the weld and nearby HAZ. Moreover, as it is shown in I-shaped columns (Fig. 12(b)), the highest stresses shift

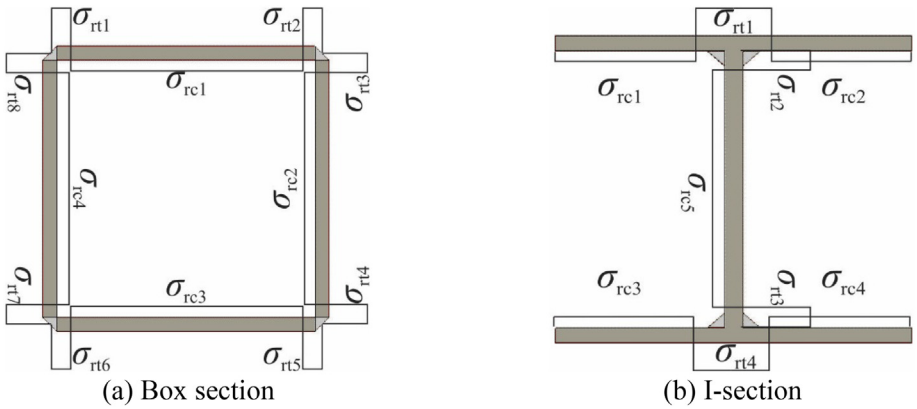

Fig. 10. Characterised residual stress distribution for fabricated columns.

Table 4
Average residual stress of fabricated UHSS box columns.

Specimens	Tensile residual stresses (MPa)								Compressive residual stresses (MPa)			
	σ_{rt1}	σ_{rt2}	σ_{rt3}	σ_{rt4}	σ_{rt5}	σ_{rt6}	σ_{rt7}	σ_{rt8}	σ_{rc1}	σ_{rc2}	σ_{rc3}	σ_{rc4}
B-1	733	747	751	740	742	702	757	702	−125	−101	−103	−111
B-2	732	750	717	756	800	806	723	741	−56	−60	−55	−50

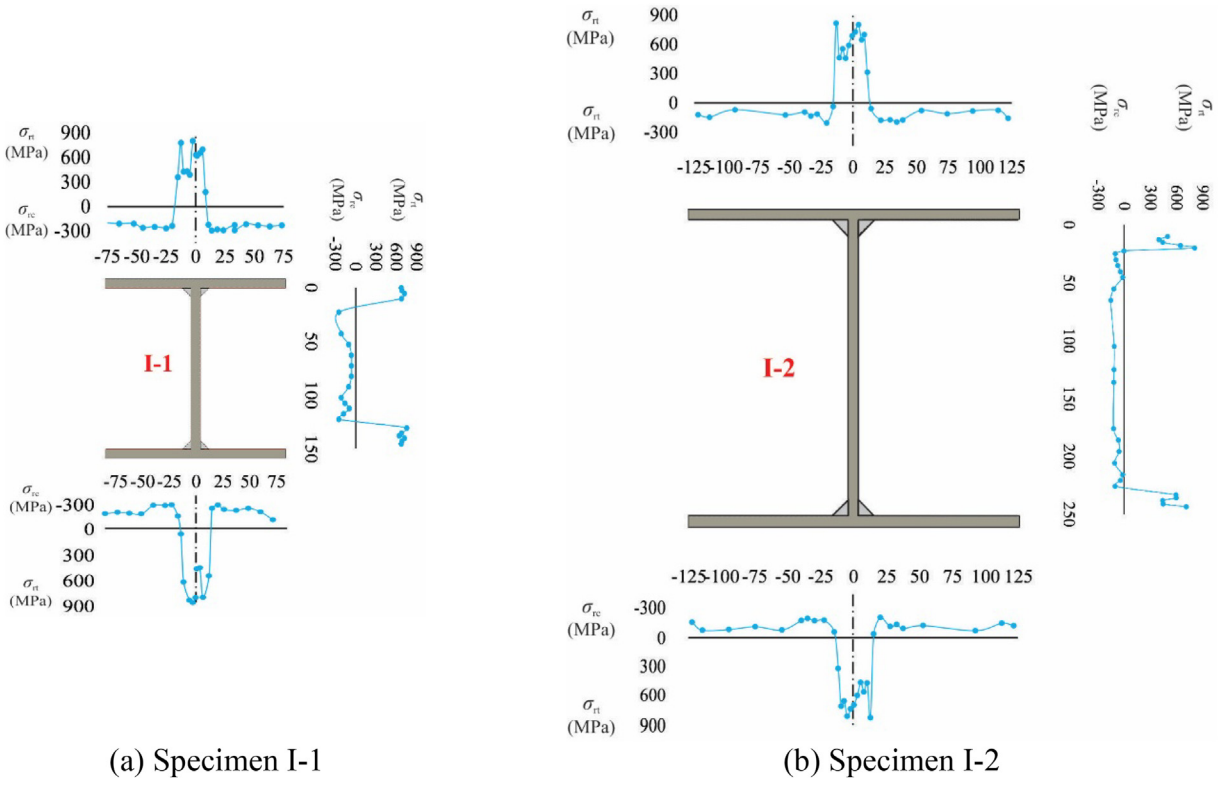

Fig. 11. Longitudinal residual stresses of fabricated UHSS I-shaped columns.

towards the second weld, as it provided localised heat treatment for first weld. The highest tensile residual stresses in the box columns are found in the HAZ which is due to the geometry of that weld and high constraints at the weld toes. In addition, for Specimen I-1, the tensile residual stress at the centre of the flange plate (Point A in Fig. 12(b)) is slightly lower than that at the end of the web plate (Point B in Fig. 12(b)), which is mainly due to the larger cooling areas of the flange plates. This phenomenon might be more significant with an increase in the thickness of the flange plate.

4.5. Effects of column dimension and plate thickness

The Standing Committee on Structural Safety (SCOSS) recently reported a series of effects that can be induced when large-scale structures with very thick structural members were used. Specifically, very thick plates (>100 mm) are vulnerable to brittle fracture and cracking from through-thickness stressing, which is partly related to the welding procedure and residual stresses [51]. It is therefore imperative to comprehensively investigate the residual stress distributions for large-scale welded columns. In the present study, both box and I-shaped columns were fabricated with 5 mm thick UHSS only, the authors therefore combined the test results obtained from [27–31,38] for the following analysis.

Table 5
Average residual stress of fabricated UHSS I-shaped columns.

Specimens	Tensile residual stresses (MPa)				Compressive residual stresses (MPa)				
	σ_{rt1}	σ_{rt2}	σ_{rt3}	σ_{rt4}	σ_{rc1}	σ_{rc2}	σ_{rc3}	σ_{rc4}	σ_{rc5}
I-1	716	686	680	702	−226	−243	−241	−251	−161
I-2	712	711	725	708	−104	−113	−106	−111	−88

Fig. 13 presents the relationships of normalised compressive (σ_{rc}/f_y) and tensile (σ_{rt}/f_y) residual stress against the width-to-thickness ratio for box and I-shaped columns. It is noteworthy that for each plate thickness, test results from different studies are utilised. The test results obtained from the neutron diffraction method are denoted with solid points, whilst other results obtained through the sectioning method are represented with hollow points.

As observed in Figs. 13(a–b), the normalised tensile residual stress (σ_{rt}/f_y) of box column component plate is independent of the width-to-thickness ratio. However, an increasing trend of the normalised tensile residual stress (σ_{rt}/f_y) can be observed when thicker steel plates are used. This is mainly due to the fact that thicker plates require more welding passes during the fabrication process, which inevitably results in higher total heat input and consequently higher stress. In contrast, the normalised compressive residual stress (σ_{rc}/f_y) is inversely

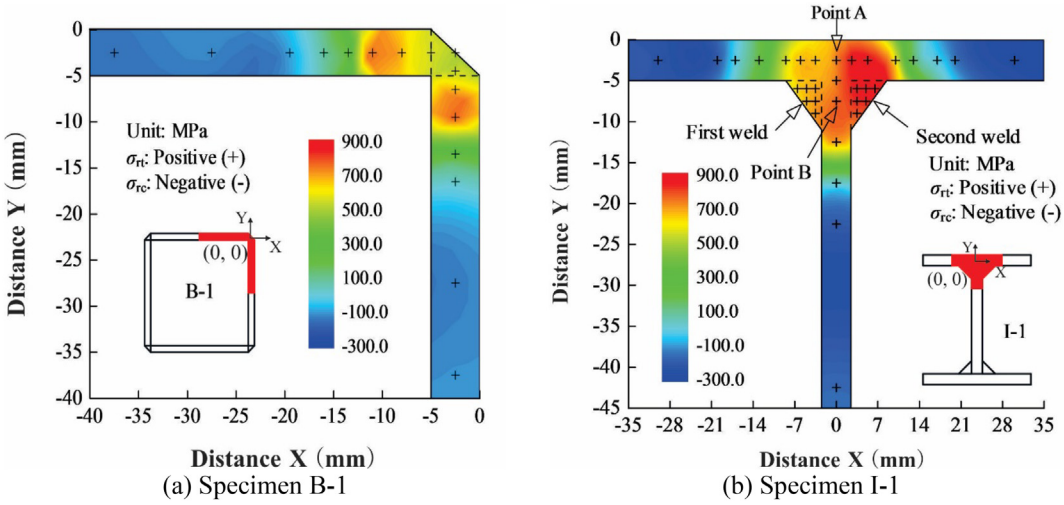

Fig. 12. Longitudinal residual stresses of the weld bead.

proportional to the width-to-thickness ratio. However, the effects of plate thickness on compressive residual stress (σ_{rc}/f_y) is still unclear as various test results are not consistent. Moreover, the shaded area in Fig. 13(b) indicates the ranges of width-to-thickness ratios for box columns that are readily available in the current market. It can be clearly observed that a conservative limit of normalised compressive residual stress ($\sigma_{rc}/f_y = 0.3$) can be used for most of the HSS and UHSS box columns.

Similarly, Fig. 13(c–d) illustrate the effects of plate thickness on residual stress for HSS and UHSS I-shaped columns. It should be noted that only the flange plates of I-shaped columns are selected herein for analysis, since the web plates can be treated as similar to the component plates of box columns. Once again, the normalised tensile residual stress (σ_{rtf}/f_y) shows no significant correlation with the width-to-thickness ratio. Nevertheless, the flange plates of I-shaped columns display a clear indication that thicker flange plates can lower the normalised compressive residual stress (σ_{rcf}/f_y) with a given width-to-thickness ratio. If the flange plates are designed around the slenderness limit ($4 < b_{tf}/t_f < 12$), which are also the sizes of products readily available for engineering practice (shaded area), a conservative normalised compressive residual stress ($\sigma_{rc}/f_y = 0.3$) can still be applied with sufficient confidence.

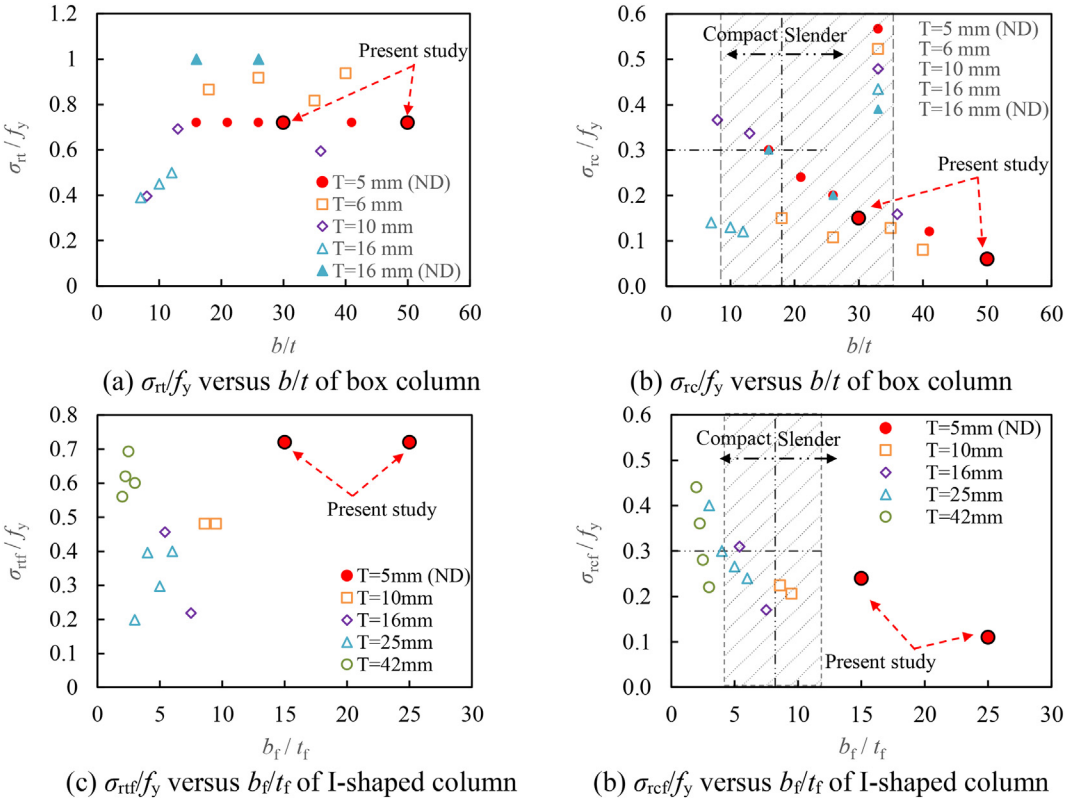

Fig. 13. Effects of column dimension and plate thickness on the magnitude of residual stress.

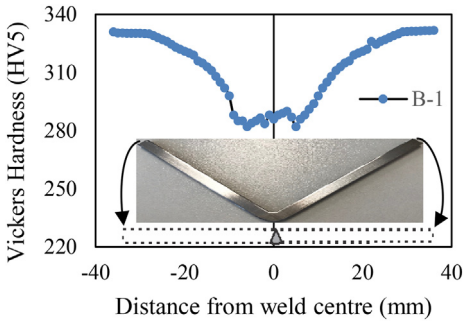

Fig. 14. Hardness measurements of the welded sections.

4.6. Effects of weld quality

The weld quality is not only of paramount importance for the design of steel structures, but also affects the measurement of residual stress. Investigations on the weld quality of the measured specimens have been performed. The hardness tests were conducted on part of the specimen B-1 with DuraScan-70 test machine according to AS/NZS 1817.1 [52]. Prior to the hardness tests, the specimens for measurement were polished and cleaned. Vickers scale (HV) with a 5 kg indentation load was applied on the surfaces of the measured points for 10s. The hardness measurements commenced from the weld and extended to each component plate for 30 mm with a spacing of 1 mm. The measured hardness values of the selected sample are shown in Fig. 14. The hardness at the base metal region is around 330 HV and gradually decreased towards the welds, which is recorded as 286 HV. The minimum hardness was identified at the location close to the HAZ (282 HV), which is around 85% of the base metal. Similar to the study reported by [53], nearly uniform hardness values are obtained over the weld regions, which are lower than those at the base metals and slightly higher than those at the HAZs. This difference comes mainly from two aspects. The first aspect is the utilisation of undermatched weld filler. The weld filler used for UHSS column is normally one or two categories lower than the base metal, which aims to lower the risk of cold cracking and lamellar tearing. Secondly, the tensile residual stresses can also lower the hardness to some extent. The maximum tensile residual stresses of the fabricated columns normally occur at the HAZs (Figs. 9 and 11), which demonstrates that the minimum hardness values can be observed in the same regions. Overall, the nearly uniform hardness values over the weld regions indicate that the quality of welding is assured during the fabrication process. The obtained residual stresses in the present study can therefore be properly utilised for the establishment of analytical models.

5. Analytical model for engineering practice

5.1. Existing models for fabricated HSS columns

Over the past decade, various analytical models concerning the box and I-shaped columns' residual stress distributions were developed to facilitate the use of structural engineers [23–32]. Most of the previous experimental studies utilised sectioning and hole-drilling method to obtain the averaged tensile residual stress for HSS box sections of different wall thickness, as shown in Fig. 15(a). As observed, the obtained averaged tensile residual stress from different studies ranges from $0.5f_y$ to $0.7f_y$. However, no obvious correlation between the plate thickness and averaged tensile residual stress can be observed. Most of the

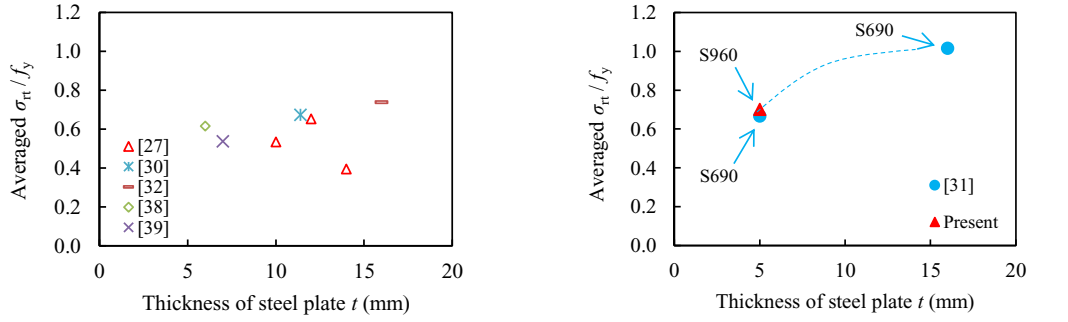

(a) Sectioning method from previous studies (b) Neutron diffraction method in present study

Fig. 15. Correlation between plate thickness and averaged tensile residual stress.

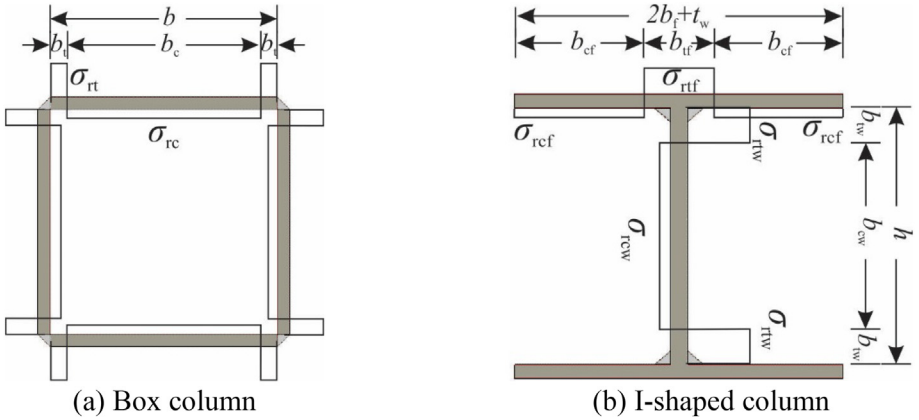

(a) Box column (b) I-shaped column

Fig. 16. Simplified design model for fabricated HSS and UHSS columns.

Table 6
Residual stress distributions of UHSS box and I-shaped columns.

Plates	σ_{rt} ($\sigma_{rtw}/\sigma_{rtf}$)	b_t (b_{tw}/b_{tf})	b_c (b_{cw}/b_{cf})	σ_{rc} ($\sigma_{rcw}/\sigma_{rcf}$)
Box column (*component plate*)	$\sigma_{rt}/f_y = 0.3\ln(t) + 0.3$	$b_t = 6.5\ln(t) + 2$	$b_c = b\text{-}2b_t$	$\sigma_{rc} = 2\sigma_{rt}b_t/b_c$
I-shaped column (*web*)	$\sigma_{rtw}/f_y = 0.3\ln(t_w) + 0.3$	$b_{tw} = 8\ln(t) + 2$	$b_{cw} = h\text{-}2b_{tw}$	$\sigma_{rcw} = 2\sigma_{rtw}b_{tw}/b_{cw}$
I- shaped column (*flange*)	$\sigma_{rtf}/f_y = 0.3\ln(t_f) + 0.3$	$b_{tf} = 20\ln(t) + 2$	$b_{cf} = (2b_f + t_w\text{-}b_{tf})/2$	$\sigma_{rcf} = \sigma_{rtf}b_{tf}/(2b_{cf})$

previous studies therefore simply assumed the averaged tensile residual stresses near the weld to be as high as their yield stresses for conservativeness. The present study and previous work by [31] utilise the neutron diffraction method to obtain the averaged tensile residual stress (Fig. 15(b)), which clearly indicates that the averaged tensile residual stress is increased with an increase in the plate thickness. A natural logarithm equation is thus proposed accordingly.

5.2. Proposed models for HSS and UHSS columns

The present experimental results and those reported by [28] are used for the identification of tensile residual stress. Specifically, the normalised tensile residual stress (σ_{rt}/f_y) of a HSS and UHSS box column component plate is expressed as a function of plate thickness (t) only, as shown in Fig. 16 and Eq. [9]. This phenomenon has been reported in many of the previous studies [30,34].

$$\frac{\sigma_{rt}}{f_y} = 0.3\ \ln(t) + 0.3 \le 1.0 \tag{9}$$

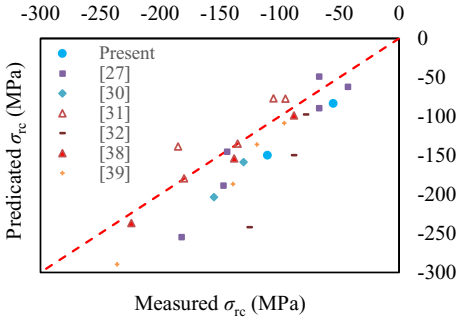

Fig. 17. Validation of the design model in terms of compressive residual stress for HSS and UHSS box column.

In addition, the width of plate where the tensile residual stresses exist (b_t) can be predicted with a simplified Eq. (10):

$$b_t = 6.5\ \ln(t) + 2 \tag{10}$$

The width of plate where the compressive residual stresses induced and the magnitude of compressive residual stresses can be obtained through Eqs. [11,12]:

$$b_c = b - 2b_t \tag{11}$$

$$\sigma_{rc} = 2\sigma_{rt}b_t/b_c \tag{12}$$

The normalised tensile residual stress (σ_{rt}/f_y) for HSS and UHSS I-shaped column web plates and flange plates are identical to the box column component plates. However, the equations that are used to calculate the width of tensile residual stresses for I-shaped columns need to be adapted slightly, owing to the increased heat input from two welding passes.

$$b_{tw} = 8\ \ln(t) + 2 \tag{13}$$

$$b_{tf} = 20\ \ln(t) + 2 \tag{14}$$

The proposed simplified equations for box and I-shaped columns' residual stresses are summarised in Table 6.

5.3. Validation of the design models

The compressive residual stresses are relatively constant over a large proportion of the base metal, the measurements of compressive residual stresses through conventional sectioning or hole-drilling methods can also be accurate. Therefore, the developed analytical models in terms of compressive residual stresses are validated with present and previous experimental results, which are measured with both destructive and non-destructive methods, as illustrated in Figs. (17–18). It can be seen that most of the predicted compressive residual stresses of HSS and UHSS box and I-shaped columns are greater than the actual measured values, which meant that the proposed simplified model can be safely adopted for design purposes.

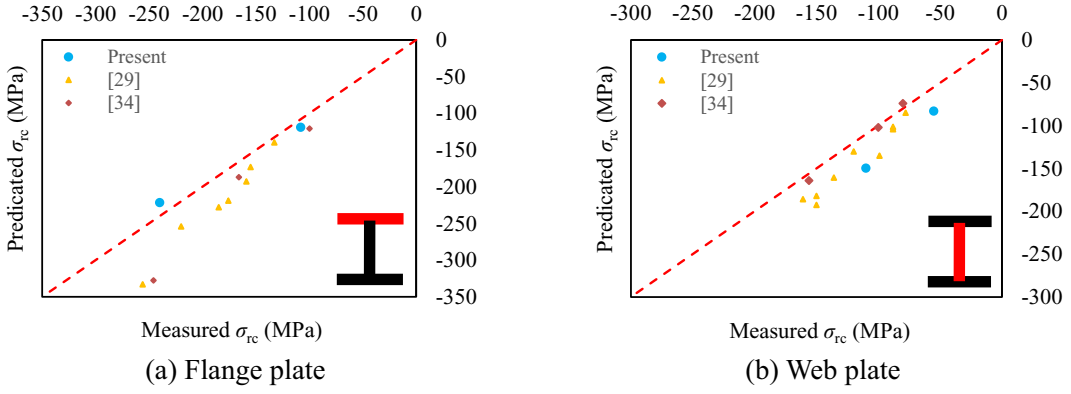

Fig. 18. Validation of the design model in terms of compressive residual stress for HSS and UHSS I-shaped columns.

6. Conclusions

The residual stresses of two box and two I-shaped columns made of UHSS plates have been successfully measured with the neutron diffraction method. According to the measurements, the residual stress distributions for UHSS box and I-shaped columns have been identified. The influences of column dimension and plate thickness on the magnitude of residual stress are discussed and further study is recommended. The weld quality has been investigated prior to the development of analytical models. Based on this study, the following conclusions can be drawn:

- The neutron diffraction method is well suited for residual stresses measurements of fabricated steel columns. Further tests on large-scale fabricated columns are recommended, through which the effects of very thick plates (thickness around 50 mm) on the residual stresses can be investigated. Cross correlation with other residual stress techniques is also encouraged.
- The tensile residual stress (σ_{rt}/f_y) of thin-walled box and I-shaped columns near the welds is around 0.7. The previous assumption of $\sigma_{rt}/f_y = 1.0$ leads to over-conservative design. The tensile residual stresses (σ_{rt}/f_y) have no correlation with the width-to-thickness ratio, but tend to increase with an increase in the plate thickness.
- The compressive residual stresses (σ_{rc}/f_y) of the measured thin-walled box and I-shaped columns are smaller than 0.3, and this value increases with a decrease in the width-to-thickness ratio. For the fabricated HSS and UHSS columns that are readily available in the current market, the compressive residual stresses (σ_{rc}/f_y) can be conservatively limited to 0.3 for design purposes.
- The proposed simplified equations for predicting the tensile and compressive residual stresses of fabricated HSS and UHSS columns take into account the plate thickness only. Comparison results indicate that the proposed simplified equations are safe to be adopted by the engineering practice.
- The additional tensile residual stresses at the edges of I-shaped column flange plates are not found due to waterjet cutting process, which is significantly different from those with flame cutting. It is recommended to investigate the effects of various cutting methods, such as flame cutting, waterjet cutting and laser cutting, on the residual stress distribution pattern in future.
- The tensile stress within the vicinity of the weld can be reduced with the change to the welding process to minimise heat input, investigation of laser welding processes are recommended.

Declaration of Competing Interest

None.

Acknowledgement

The research described in this paper was supported by funding from Australian Nuclear Science and Technology Organisation (ANSTO) through Proposal 6851. The first author was supported by the Australian Research Council (ARC) under its Discovery Scheme (Project No: DP170100001).

References

[1] J.L. Ma, T.M. Chan, B. Young, Design of cold-formed high-strength steel tubular stub columns, J. Struct. Eng. 144 (6) (2018), 04018063.
[2] B. Uy, Strength of short concrete filled high strength steel box columns, J. Constr. Steel Res. 57 (2001) 113–134.
[3] G. Shi, H. Ban, F.S.K. Bijlaard, Tests and numerical study of ultra-high strength steel columns with end restraints, J. Constr. Steel Res. 70 (2012) 236–247.
[4] H. Ban, G. Shi, Y.J. Shi, M.A. Bradford, Experimental investigation of the overall buckling behaviour of 960 MPa high strength steel columns, J. Constr. Steel Res. 88 (2013) 256–266.
[5] Y.B. Wang, G.Q. Li, S.W. Chen, F.F. Sun, Experimental and numerical study on the behaviour of axially compressed high strength steel box-columns, Eng. Struct. 58 (2014) 79–91.
[6] T.J. Li, G.Q. Li, S.L. Chan, Y.B. Wang, Behaviour of Q690 high-strength steel columns: part 1: experimental investigation, J. Constr. Steel Res. 123 (2016) 18–30.
[7] T.Y. Ma, Y.F. Hu, X. Liu, G.Q. Li, K.F. Chung, Experimental investigation into high strength Q690 steel welded H-sections under combined compression and bending, J. Constr. Steel Res. 138 (2017) 449–462.
[8] K.J.R. Rasmussen, G.J. Hancock, Tests of high strength steel columns, J. Constr. Steel Res. 34 (1) (1995) 27–52.
[9] B. Uy, Axial compressive strength of short steel and composite columns fabricated with high strength steel plate, Struct. Eng. Mech. 1 (2) (2001) 1–15.
[10] M. Mursi, B. Uy, Strength of slender concrete filled high strength steel box columns, J. Constr. Steel Res. 60 (2004) 1825–1848.
[11] F. Aslani, B. Uy, Z. Tao, F. Mashiri, Behaviour and design of composite columns incorporating compact high-strength steel plates, J. Constr. Steel Res. 107 (2015) 94–110.
[12] Y. Du, Z. Chen, J.Y.R. Liew, M.X. Xiong, Rectangular concrete-filled steel tubular beam-columns using high-strength steel: experiments and design, J. Constr. Steel Res. 131 (2017) 1–18.
[13] M.X. Xiong, D.X. Xiong, J.Y.R. Liew, Axial performance of short concrete filled steel tubes with high- and ultra-high- strength materials, Eng. Struct. 136 (2017) 494–510.
[14] K.A. Skalomenos, K. Hayashi, R. Nishi, H. Inamasu, M. Nakashima, Experimental behavior of concrete-filled steel tube columns using ultrahigh-strength steel, J. Struct. Eng. 142 (9) (2016), 04016057.
[15] Z. Lai, A.H. Varma, High-strength rectangular CFT members: database, modelling, and design of short columns, J. Struct. Eng. 144 (5) (2018), 04018036.
[16] Z. Huang, D. Li, B. Uy, H.T. Thai, C. Hou, Local and post-local buckling of fabricated high strength steel and composite columns, J. Constr. Steel Res. 154 (2019) 235–249.
[17] D. Li, Z. Huang, B. Uy, H.T. Thai, C. Hou, Slenderness limits for fabricated S960 ultra-high-strength steel and composite columns, J. Constr. Steel Res. 159 (2019) 109–121.
[18] C.C. Chou, S.C. Wu, Cyclic lateral load test and finite element analysis of high-strength concrete-filled steel box columns under high axial compression, Eng. Struct. 189 (15) (2019) 89–99.
[19] C. Acevedo, A. Nussbaumer, Effect of tensile residual stresses on fatigue crack growth and S–N curves in tubular joints loaded in compression, Int. J. Fatigue 36 (1) (2012) 171–180.
[20] C. Acevedo, A. Evans, A. Nussbaumer, Neutron diffraction investigations on residual stresses contributing to the fatigue crack growth in ferritic steel tubular bridges, Int. J. Pres. Ves. Pip. 95 (2012) 31–38.
[21] J.W.H. Price, A.M. Paradowska, S. Joshi, T. Finlayson, Residual stresses measurement by neutron diffraction and theoretical estimation in a single weld bead, Int. J. Pres. Ves. Pip. 83 (5) (2006) 381–387.
[22] H. Alipooramirabad, A.M. Paradowska, R. Ghomashchi, M. Reid, Investigating the effects of welding process on residual stresses, microstructure and mechanical properties in HSLA steel welds, J. Manuf. Process. 28 (1) (2017) 70–81.
[23] P.J. Withers, Residual stress and its role in failure, Rep. Prog. Phys. 70 (2007).
[24] P.J. Withers, H.K.D.H. Bhadeshia, Residual stress Part 1-Measurement techniques, Mater. Sci. Technol. 17 (2001) 355–365.
[25] N.S. Rossini, M. Dassisti, K.Y. Benyounis, A.G. Olabi, Methods of measuring residual stresses in components, Mater. Des. 35 (2012) 572–588.
[26] P. Mikula, M. Vrana, P. Lukas, Power of Bragg diffraction optics for high-resolution neutron diffractometers for strain/stress scanning, Proceedings of Measurement of Residual Stress in Materials Using Neutrons, October 13–17, Vienna, 2003.
[27] H. Ban, G. Shi, Y. Shi, Y. Wang, Residual stress of 460 MPa high strength steel welded box section: experimental investigation and modelling, Thin-Walled Struct. 64 (2013) 73–82.
[28] B. Yang, S. Nie, G. Xiong, Y. Hu, J. Bai, W. Zhang, G. Dai, Residual stresses in welded I-shaped sections fabricated from Q460GJ structural steel plates, J. Constr. Steel Res. 122 (2016) 261–273.
[29] B. Yang, Q. Zhu, S. Nie, M. Elchalakani, G. Xiong, Experimental and model investigation on residual stresses in Q460GJ thick-walled I-shaped sections, J. Constr. Steel Res. 145 (2018) 489–503.
[30] T.J. Li, G.Q. Li, Y.B. Wang, Residual stress tests of welded Q690 high-strength steel box- and H-sections, J. Constr. Steel Res. 115 (2015) 283–289.
[31] M. Khan, A. Paradowska, B. Uy, F. Mashiri, Z. Tao, Residual stresses in high strength steel welded box sections, J. Constr. Steel Res. 116 (2016) 55–64.
[32] J. Jiang, S.P. Chiew, C.K. Lee, P.L.Y. Tiong, An experimental study on residual stresses of high strength steel box columns, J. Constr. Steel Res. 130 (2017) 12–21.
[33] H. Fang, T.M. Chan, B. Young, Material properties and residual stresses of octagonal high strength steel hollow sections, J. Constr. Steel Res. 148 (2018) 479–490.
[34] Y.B. Wang, G.Q. Li, S.W. Chen, Residual stresses in welded flame-cut high strength steel H-sections, J. Constr. Steel Res. 79 (2012) 159–165.
[35] R.C. Spoorenberg, H.H. Snijder, L.G. Cajot, M.S. May, Experimental investigation on residual stresses in heavy wide flange QST steel sections, J. Constr. Steel Res. 89 (2013) 63–74.
[36] S.C. Kang, K.S. Kim, J.K. Lee, Experimental Investigation of Residual Stresses in HSB800 Structures by the Sectioning Method, IABSE-IASS, London, 2011.
[37] M. Abambres, W.M. Quach, Residual stresses in steel members: a review of available analytical expressions, Int. J. Struct. Integr. 7 (1) (2016) 70–94.
[38] B. Somodi, B. Kovesdi, Residual stress measurements on welded square box sections using steel grades of S235–S960, Thin-Walled Struct. 123 (2018) 142–154.

[39] X. Cao, Y. Xu, M. Wang, G. Zhao, L. Gu, Z. Kong, Experimental study on the residual stresses of 800 MPa high strength steel welded box sections, J. Constr. Steel Res. 148 (2018) 720–727.
[40] H. Ban, G. Shi, Y. Shi, Experimental study on residual stress in 960MPa high strength steel welded box sections and unified model, Tumu Gongcheng Xuebao/China Civil Eng. J. 46 (11) (2013) 63–69.
[41] W.L. Bragg, The diffraction of short electromagnetic waves by a crystal, Proc. Camb. Philos. Soc. 17 (1912) 43–57.
[42] A.M. Paradowska, J.W.H. Price, B. Kerezsi, P. Dayawansa, X.L. Zhao, Stress relieving and its effect on life of welded tubular joints, Eng. Fail. Anal. 14 (2010) 320–327.
[43] A. Paradowska, Investigation of Residual Stress in Steel Welds Using Neutron and Synchrotron Diffraction, Ph.D Thesis Monash University, Australia, 2007.
[44] C. Ohms, R.C. Wimpory, D.E. Katsareas, A.G. Youtsos, NET TG1: residual stress assessment by neutron diffraction and finite element modelling on a single bead weld on a steel plate, Int. J. Pres. Ves. Pip. 86 (2009) 63–72.
[45] M.T. Hutchings, P.J. Withers, T.M. Holden, T. Lorentzen, Introduction to the Characterization of Residual Stress by Neutron Diffraction, Taylor & Francis, 2005 (ISBN 0–415–31000-8).
[46] J.R. Taylor, An Introduction to Error Analysis: The Study of Uncertainties in Physical Measurements, 2nd edn University Science Books, Sausalito, Calif, 1997.
[47] A.M. Paradowska, J.W.H. Price, T.R. Finlayson, U. Lienert, R. Ibrahim, Comparison of neutron and synchrotron diffraction measurements of residual stress in bead-on-plate weldments, J. Press. Vessel. Technol. 132 (1) (2010) 011502.
[48] J. James, J. Santisteban, L. Edwards, M. Daymond, A virtual laboratory for neutron and synchrotron strain scanning, Phys. B Condens. Matter 350 (Supplement 1–3) (2004)(E743–E746 ISSN 0921–4526, proceedings of the Third European Conference on Neutron Scattering).
[49] A. Paradowska, J. Price, R. Ibrahim, T. Finlayson, R. Blevins, M. Ripley, Residual stress measurements by neutron diffraction in multi-bead welding, Phys. B Condens. Matter 2 (0) (2006) 385–386(890–893, ISSN 0921–4526, proceedings of the Eighth International Conference on Neutron Scattering).
[50] Australian Standard AS 1391, Metallic Materials-Tensile Testing at Ambient Temperature, Standards Australia, 2007.
[51] Standing Committee on Structural Safety, SCOSS alert-effects of scale, November 2018.
[52] Australian/New Zealand Standard AS/NZS 1817.1, Metallic Materials-Vickers Hardness Test Method 1: Test Method, 2003.
[53] B. Mvola, P. Kah, J. Martikainen, R. Suoranta, Dissimilar high-strength steels: fusion welded joints, mismatches, and challenges, Rev. Adv. Mater. Sci. 44 (2016) 146–159.